

# Non-Gaussianity analysis on local morphological measures of WMAP data

Y. Wiaux<sup>1</sup>, P. Vielva<sup>2</sup>, R. B. Barreiro<sup>2</sup>, E. Martínez-González<sup>2</sup>, P. Vandergheynst<sup>1</sup>

<sup>1</sup>*Signal Processing Institute, Ecole Polytechnique Fédérale de Lausanne (EPFL), CH-1015 Lausanne, Switzerland*

*E-mails : yves.wiaux@epfl.ch, pierre.vandergheynst@epfl.ch*

<sup>2</sup>*Instituto de Física de Cantabria (CSIC - UC), 39005 Santander, Spain*

*E-mails : vielva@ifca.unican.es, barreiro@ifca.unican.es, martinez@ifca.unican.es*

1 February 2008

## ABSTRACT

The decomposition of a signal on the sphere with the steerable wavelet constructed from the second Gaussian derivative gives access to the orientation, signed-intensity, and elongation of the signal's local features. In the present work, the non-Gaussianity of the WMAP temperature data of the cosmic microwave background (CMB) is analyzed in terms of the first four moments of the statistically isotropic random fields associated with these local morphological measures, at wavelet scales corresponding to angular sizes between  $27.5'$  and  $30^\circ$  on the celestial sphere. While no detection is made neither in the orientation analysis nor in the elongation analysis, a strong detection is made in the excess kurtosis of the signed-intensity of the WMAP data. The non-Gaussianity is observed with a significance level below 0.5% at a wavelet scale corresponding to an angular size around  $10^\circ$ , and confirmed at neighbour scales. This supports a previous detection of an excess of kurtosis in the wavelet coefficient of the WMAP data with the axisymmetric Mexican hat wavelet (Vielva et al. 2004). Instrumental noise and foreground emissions are not likely to be at the origin of the excess of kurtosis. Large-scale modulations of the CMB related to some unknown systematics are rejected as possible origins of the detection. The observed non-Gaussianity may therefore probably be imputed to the CMB itself, thereby questioning the basic inflationary scenario upon which the present concordance cosmological model relies. Taking the CMB temperature angular power spectrum of the concordance cosmological model at face value, further analysis also suggests that this non-Gaussianity is not confined to the directions on the celestial sphere with an anomalous signed-intensity.

**Key words:** methods: data analysis, techniques: image processing, cosmology: observations, cosmic microwave background

## 1 INTRODUCTION

Among other cosmological observations, the recent data of the cosmic microwave background, in particular those released by the Wilkinson Microwave Anisotropy Probe (WMAP) satellite experiment, have played a central role in defining a concordance model highlighting a flat  $\Lambda$ CDM Universe with a primordial phase of inflation (Bennett et al. 2003; Spergel et al. 2003; Hinshaw et al. 2007; Spergel et al. 2007). In that framework, the flat Universe is filled in with cold dark matter (CDM) and dark energy in the form of a cosmological constant ( $\Lambda$ ), in addition to the standard baryonic and electromagnetic components. The cosmological principle is assumed, which postulates global homogeneity and isotropy. In the basic inflationary scenario considered, the large scale structure and the cosmic microwave back-

ground fluctuations are also assumed to arise from Gaussian quantum energy density perturbations around the homogeneous and isotropic background during the inflationary phase. The cosmological parameters of the concordance cosmological model are determined with a precision of the order of several percent, but the hypotheses on which the model relies need to be thoroughly challenged.

In that context, the CMB constitutes a realization of a random field on the sphere. The cosmological principle and the basic inflationary scenario respectively imply the statistical isotropy and the Gaussianity of this random field. These basic hypotheses of the concordance cosmological model may consequently be questioned through the CMB analysis.

The statistical isotropy of the CMB tempera-

ture field has already been largely questioned in the analysis of the WMAP data. Firstly, a North-South asymmetry in ecliptic coordinates has been detected (Eriksen et al. 2004a,b, 2005; Hansen et al. 2004a,b; Donoghue & Donoghue 2005; Land & Magueijo 2005a; Bernui et al. 2006, 2007; Spergel et al. 2007; Eriksen et al. 2007; Monteserín et al. 2007). Secondly, an anomalous alignment of the lowest multipoles of the data was observed (de Oliveira-Costa et al. 2004; Schwarz et al. 2004; Copi et al. 2004; Katz & Weeks 2004; Bielewicz et al. 2005; Land & Magueijo 2005b, 2007; Freeman et al. 2006; Abramo et al. 2006). Finally, wavelet analyses have also reported statistical isotropy anomalies related to the signed-intensity of local CMB features, as well as anomalies related to the alignment of local CMB features toward specific directions on the celestial sphere (Wiaux et al. 2006a; Vielva et al. 2006, 2007).

The Gaussianity of the CMB temperature field has also been largely questioned in the analysis of the WMAP data. Firstly, departures from Gaussianity were detected using statistics of extrema (Larson & Wandelt 2004, 2005; Tojeiro et al. 2006), bispectra (Land & Magueijo 2005a), phase correlations (Chiang et al. 2003; Chiang & Naselsky 2006; Coles et al. 2004; Naselsky et al. 2005), Minkowski functionals (Park 2004; Eriksen et al. 2004b), and local curvature (Hansen et al. 2004a). Secondly, wavelet analyses have also reported non-Gaussian deviations. An excess of kurtosis in the wavelet coefficient of the WMAP temperature data with the axisymmetric Mexican hat wavelet on the sphere was found at wavelet scales corresponding to angular sizes on the celestial sphere around  $10^\circ$ , and localized in the southern galactic hemisphere (Vielva et al. 2004). A cold spot (*i.e.* with negative wavelet coefficients) was identified at  $(\theta, \varphi) = (147^\circ, 209^\circ)$ , with  $\theta \in [0, \pi]$  and  $\varphi \in [0, 2\pi]$  respectively standing for the co-latitude and longitude in galactic spherical coordinates, and considered to be a good candidate to explain the observed deviation. The confirmation that the cold spot is anomalous was provided, still with the axisymmetric Mexican hat wavelet, in terms of its area (Cruz et al. 2005). The detection was further confirmed with various wavelets and various statistics (Mukherjee & Wang 2004; Cayón et al. 2005; McEwen et al. 2005; Cruz et al. 2006, 2007; McEwen et al. 2006). Notice that the cold spot identified also certainly represents a departure from statistical isotropy, in terms of a North-South asymmetry in galactic coordinates.

By essence, wavelet analyses present the particular advantage of probing, not only the scale but also the localization of the features constituting the CMB on the celestial sphere (Wiaux et al. 2005). Steerable wavelets also provide morphological measures of the local features, such as orientation, signed-intensity, or elongation (McEwen et al. 2007), at a low computational cost (Wiaux et al. 2006b). They were used to probe the statistical isotropy of the WMAP CMB temperature data in the previously quoted signed-intensity and alignment analyses. They were also used to probe the Integrated Sachs-Wolfe effect through the correlation of WMAP data and large scale structure data (McEwen et al. 2007). In the present work, a further insight into the CMB temperature non-Gaussianity is provided through a steerable wavelet analysis of the WMAP data.

In Section 2, we present the methodology adopted. In

Section 3, we present the results of the WMAP data analysis. In Section 4, we study systematic effects as a possible origin of the detections. In Section 5, we discuss the origin of our detection and its detailed interpretation. We finally conclude in Section 6.

## 2 METHODOLOGY

In this section, we firstly recall the formalism for the analysis of signals on the sphere with steerable wavelets, as well as the local morphological measures of orientation, signed-intensity, and elongation, defined from the steerable wavelet constructed from the second Gaussian derivative. Secondly, we explicitly describe the statistics for the non-Gaussianity analysis on the random fields associated with the local morphological measures of the CMB temperature field. These statistics are simply the first four moments of the random fields considered.

### 2.1 Steerable wavelets and morphological measures

We consider the three-dimensional Cartesian coordinate system  $(o, o\hat{x}, o\hat{y}, o\hat{z})$  centered on the unit sphere, and where the direction  $o\hat{z}$  identifies the North pole. Any point  $\omega$  on the sphere is identified by its corresponding spherical coordinates  $(\theta, \varphi)$ , where  $\theta \in [0, \pi]$  stands for the co-latitude, and  $\varphi \in [0, 2\pi]$  for the longitude.

Firstly, we briefly summarize the formalism of steerable wavelets on the sphere  $S^2$  (Wiaux et al. 2005). Any filter invariant under rotation around itself is said to be axisymmetric. By definition, any non-axisymmetric, or directional, filter  $\Psi$  is steerable if a rotation by  $\chi \in [0, 2\pi]$  around itself may be expressed in terms of a finite linear combination of  $M$  non-rotated basis filters  $\Psi_m$ :

$$\Psi_\chi(\omega) = \sum_{m=1}^M k_m(\chi) \Psi_m(\omega), \quad (1)$$

where the weights  $k_m(\chi)$ , with  $1 \leq m \leq M$ , are called interpolation functions. The analysis of a signal  $F$  with a given wavelet  $\Psi$  simply defines a set of wavelet coefficients  $W_\Psi^F(\omega_0, \chi, a)$ , which result from the directional correlation between  $F$  and the wavelet dilated at any scale  $a$ ,  $\Psi_a$ . In other words these wavelet coefficients are defined by the scalar product between the signal and the wavelet dilated at scale  $a$ , rotated around itself by  $\chi$ , and translated at any point  $\omega_0$  on the sphere, also denoted  $\Psi_{\omega_0, \chi, a}$ :

$$W_\Psi^F(\omega_0, \chi, a) = \langle \Psi_{\omega_0, \chi, a} | F \rangle = \int_{S^2} d\Omega \Psi_{\omega_0, \chi, a}^*(\omega) F(\omega). \quad (2)$$

The  $*$  denotes complex conjugation. The wavelet coefficients of a signal therefore characterize the signal at each scale  $a$ , orientation  $\chi$ , and position  $\omega_0$ .

In the present work, we consider the second Gaussian derivative wavelet (2GD),  $\Psi^{\partial_x^2(gau)}$ , which is obtained by a stereographic projection of the second derivative in direction  $\hat{x}$  of a Gaussian in the tangent plane at the North pole. The filter obtained is a steerable wavelet on the sphere which may be rotated in terms of three basis filters ( $M = 3$ ): the second derivative in the direction  $\hat{x}$  itself, the second derivative in the direction  $\hat{y}$ , and the cross-derivative. Notice that

the value of the scale  $a$  identifies with the dispersion of the Gaussian in units of  $2 \tan(\theta/2)$ . The angular size of the 2GD is defined as twice the half-width of the wavelet, where the half-width is defined by  $\theta_{hw} = 2 \arctan(a/2)$ , which is closely approximated by  $a$  at small scales.

Secondly, we recall that the 2GD gives access to three local morphological measures of orientation, signed-intensity, and elongation (McEwen et al. 2007). By linearity, the relation of steerability (1) is automatically transferred on the wavelet coefficients of  $F$ . Consequently, at each scale  $a$  and at each position  $\omega_0$ , the orientation  $\chi_0(\omega_0, a)$  that maximizes the absolute value of the wavelet coefficient, can easily be computed, with an infinite theoretical precision. It corresponds to the local orientation at which the wavelet best matches the local feature of the signal. As the 2GD is invariant under rotation around itself by  $\pi$ , orientations may arbitrarily be constrained in a range of length  $\pi$ , and as the 2GD oscillates in the tangent direction  $\hat{x}$ , it actually detects features aligned along the tangent direction  $\hat{y}$ . The local orientation of the feature itself,  $D^F(\omega_0, a)$ , is therefore defined in terms of  $\chi_0 = \chi_0(\omega_0, a)$  as:

$$\frac{\pi}{2} \leq D^F(\omega_0, a) \equiv \chi_0 + \frac{\pi}{2} < \frac{3\pi}{2}. \quad (3)$$

The wavelet coefficient itself at scale  $a$ , position  $\omega_0$ , and in direction  $\chi_0$ , defines to so-called signed-intensity of the local feature:

$$I^F(\omega_0, a) \equiv W_{\Psi^F}^F(\omega_0, \chi_0, a). \quad (4)$$

The elongation of local features is explicitly defined by

$$0 \leq E^F(\omega_0, a) \equiv 1 - \left| \frac{W_{\Psi^F}^F(\omega_0, \chi_0 + \frac{\pi}{2}, a)}{W_{\Psi^F}^F(\omega_0, \chi_0, a)} \right| \leq 1. \quad (5)$$

Numerical tests performed on elliptical Gaussian-profile features show that this elongation measure increases monotonously in the range  $[0, 1]$  with the intrinsic eccentricity  $e \in [0, 1]$  of the features. While it is possible to define alternative elongation measures, these numerical tests also indicate that the chosen definition is not an arbitrary measure of the non-axisymmetry of local features, but represents a rough estimate of the eccentricity of a Gaussian-profile local feature.

In summary, the analysis of signals with steerable wavelets is interesting in several respects. Firstly, the wavelet decomposition enables one to identify the scales  $a$  of the physical processes which define the local feature of the signal at each point  $\omega_0$ . Secondly, the steerability theoretically gives access to local morphological measures. For the 2GD, the orientation, signed-intensity and elongation of local features are defined. Finally, from the computational point of view, the calculation of a directional correlation at each analysis scale is an extremely demanding task. The relation of steerability is essential to reduce the complexity of calculation of the wavelet coefficients when local orientations are considered (Wiaux et al. 2006b).

## 2.2 Statistics for non-Gaussianity

In the context of the concordance cosmological model, the CMB temperature represents a realization of a statistically isotropic and Gaussian random field on the sphere. The

WMAP data are also contaminated by noise and foreground emissions. The statistical analysis is performed by comparison of the data with simulations. The noise present in the data is simulated and the regions of the sky in which the data are too much contaminated by foreground emissions are masked, and excluded from the analysis. Typically, a non-Gaussianity analysis is performed through the evaluation of global estimators computed as simple averages on the whole part of the celestial sphere where the data are considered to be valid, explicitly assuming the statistical isotropy in the corresponding part of the sky. Any anomaly between the data and the simulations is consequently interpreted as a departure of the data from Gaussianity.

We consider the statistically isotropic real-valued random fields on the sphere associated with the local morphological measures of orientation, signed-intensity, and elongation of the CMB temperature field  $T$  at each wavelet scale  $a$ :  $X(\omega_0, a)$ , with  $X = \{D^T, I^T, E^T\}$ . The statistics estimated for the subsequent non-Gaussianity analysis are simply moments of the first four orders. The first two are the mean  $\mu^X(a) = \langle X(\omega_0, a) \rangle$ , and variance  $\sigma^X(a) = \langle [X(\omega_0, a) - \mu^X(a)]^2 \rangle^{1/2}$ . The third-order moment is the skewness  $S^X(a) = \langle [X(\omega_0, a) - \mu^X(a)]^3 \rangle / [\sigma^X(a)]^3$ . The skewness measures the asymmetry of the probability density function, and hence a deviation relative to a Gaussian distribution. Positive and negative skewnesses are respectively associated with larger right and left distribution tails. The fourth-order moment considered is the excess kurtosis  $K^X(a) = \langle [X(\omega_0, a) - \mu^X(a)]^4 \rangle / [\sigma^X(a)]^4 - 3$ . The kurtosis measures the peakedness of the probability density function relative to a Gaussian distribution. Positive and negative excess kurtoses are respectively associated with distributions more and less peaked than a Gaussian distribution. These four moments are independent of the point  $\omega_0$  because of the statistical isotropy. The corresponding estimators computed by averages over the sphere are

$$\begin{aligned} \hat{\mu}^X(a) &= \frac{1}{N_a} \sum_{i=1}^{N_a} X(\omega_0^{(i)}, a) \\ \hat{\sigma}^X(a) &= \left\{ \frac{1}{N_a} \sum_{i=1}^{N_a} [X(\omega_0^{(i)}, a) - \hat{\mu}^X(a)]^2 \right\}^{1/2} \\ \hat{S}^X(a) &= \frac{1}{N_a} \sum_{i=1}^{N_a} \left[ \frac{X(\omega_0^{(i)}, a) - \hat{\mu}^X(a)}{\hat{\sigma}^X(a)} \right]^3 \\ \hat{K}^X(a) &= \frac{1}{N_a} \sum_{i=1}^{N_a} \left[ \frac{X(\omega_0^{(i)}, a) - \hat{\mu}^X(a)}{\hat{\sigma}^X(a)} \right]^4 - 3. \quad (6) \end{aligned}$$

At each wavelet scale  $a$ ,  $N_a$  stands for the total number of valid pixels outside a given exclusion mask  $M_a$  which, by definition, identifies the pixels to be excluded from the analysis (see Subsection 3.1). The values  $\omega_0^{(i)}$  identify the center of these valid pixels.

Let us emphasize here that, even under the assumption of Gaussianity of the CMB temperature field, postulated for the simulations, none of the random fields associated with these local morphological measures at each scale is intrinsically Gaussian. This is simply due to the non-linearity of the definitions (3) for the orientation, (4) for the signed-intensity, and (5) for the elongation. In particular,

by statistical isotropy, the measure of orientation  $D^F(\omega_0, a)$  should be uniformly distributed at each point  $\omega_0$  and at each wavelet scale  $a$ .

For each local morphological measure, statistics, and wavelet scale, the value obtained for the data can be compared to the corresponding values for the simulations. The percentiles corresponding to specific cumulative probabilities  $p$  in the simulations considered are calculated for a first comparison with the value of the data. The percentile associated with  $p = 50\%$  defines the median value. Cumulative probabilities  $p = \{15.865\%, 84.135\%\}$  are considered, which formally correspond to the percentiles at one standard deviation ( $1\sigma$ ) from the mean in a Gaussian distribution. They define a first, innermost, region for the distribution of percentiles around the median value. The exact values considered reflect the maximum precision allowed by our sample of ten thousand simulations. Cumulative probabilities  $p = \{2.275\%, 97.725\%\}$  are also considered, which formally correspond to the percentiles at two standard deviations ( $2\sigma$ ) from the mean in a Gaussian distribution. They define a second, middle, region for the distribution of percentiles around the median value. Again, the exact values considered reflect the maximum precision allowed by our sample of ten thousand simulations. Cumulative probabilities  $p = \{0.5\%, 99.5\%\}$  are finally considered, defining a third, outermost, region for the distribution of percentiles around the median value. If the value of the data for a statistics at a given scale is higher (lower) than the median value obtained from the simulations, the significance level of a detection is simply defined as the fraction of simulations with a higher (lower) value than the data. The lower the significance level, the stronger the detection. Typically, in the following, a significance level below 0.5%, corresponding to values outside the outermost region for the distribution of percentiles around the median value, will be associated with a strong detection.

### 3 WMAP ANALYSIS

In this section, we firstly describe the pre-processing procedure applied to the three-year WMAP CMB temperature data, as well as to the corresponding simulations produced from the concordance cosmological model. Secondly, we expose the results of the application of the non-Gaussianity analysis defined in the previous section on the three-year WMAP co-added CMB data, notably highlighting a strong detection in the excess kurtosis of the signed-intensity.

#### 3.1 Data and simulations

Firstly, the following pre-processing procedure is applied to the three-year WMAP CMB temperature data before the non-Gaussianity analysis. The original maps of the eight WMAP radiometers at the Q, V, and W frequencies (Q1 and Q2 at 41 GHz, V1 and V2 at 61 GHz, and W1, W2, W3, and W4 at 94 GHz) are corrected for foreground emissions contamination by a template fitting technique (Spergel et al. 2007). The resulting foreground cleaned maps are available

from the NASA LAMBDA archive<sup>1</sup>. These maps are masked with the Kp0 mask (Spergel et al. 2007) that cuts the regions of brightest galactic emission around the galactic plane ( $\approx 20\%$  of the sky), as well as the brightest galactic and extragalactic point sources ( $\approx 5\%$  of the sky). Zero values are assigned to the corresponding pixels. The instrumental beam associated with the WMAP radiometers is described by an isotropic window function, and the instrumental noise is to first order Gaussian, statistically anisotropic, and uncorrelated. A map with better signal-to-noise ratio can be obtained by an optimal combination of the eight foreground cleaned and masked maps. At each pixel, this combination is obtained by weighting each map by the corresponding inverse noise variance. In order to minimize any error coming from the cosmological dipole subtraction, the dipole outside the mask is removed (Komatsu et al. 2003). This overall pre-processing procedure defines the so-called three-year WMAP co-added CMB map (Hinshaw et al. 2007), which is used in the subsequent analysis.

Secondly, ten thousand simulations of the three-year WMAP co-added CMB map are considered to compare the results of the analysis of the data to what is expected from the concordance model. Each simulation is produced as follows. Spherical harmonics coefficients of a statistically isotropic and Gaussian CMB realization are obtained from the angular power spectrum determined by the cosmological parameters of the three-year WMAP best-fit model (Spergel et al. 2007) with CAMB (Code for Anisotropies in the Microwave Background<sup>2</sup>). The observation at each of the eight WMAP radiometers of the Q, V, and W frequencies is simulated by convolving that realization in harmonic space with the corresponding isotropic window function. Each map is then transformed to pixel space at the appropriate resolution, and a Gaussian, statistically anisotropic, and uncorrelated noise realization is added with the proper variance per pixel. This provides simulations of the CMB, as seen by the eight radiometers at the different WMAP frequencies considered. The same prescriptions as those described above for the data are then applied to produce a three-year WMAP co-added CMB map.

Notice that the WMAP co-added CMB maps for the data and simulations are initially produced in HEALPix pixelization<sup>3</sup> (Górski et al. 2005) at the resolution  $N_{side} = 512$ , corresponding to maps with more than three million equal-area pixels with a spatial resolution of  $6.87'$ . For the sake of our analysis, which is applied at 17 scales of the 2GD wavelet, corresponding to angular sizes between  $27.5'$  and  $30'$ , the maps are downgraded to the resolution  $N_{side} = 256$ . This provides maps with a bit less than one million equal-area pixels with a spatial resolution of  $13.7'$ . Also notice that, in pixels close to masked regions, the result of the directional correlation of a signal with a steerable wavelet is inevitably affected by the zero values of the Kp0 mask. An exclusion mask  $M_a$  is therefore defined at each wavelet scale  $a$ , identically on the data and simulations, in order to exclude the affected pixels from the analysis (Vielva et al.

<sup>1</sup> <http://lambda.gsfc.nasa.gov/>

<sup>2</sup> <http://camb.info/>

<sup>3</sup> <http://healpix.jpl.nasa.gov/>

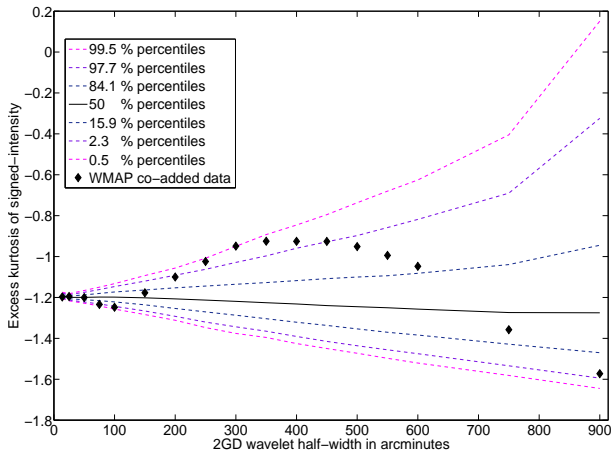


**Figure 1.** Excess kurtosis of the signed-intensity of the three-year WMAP co-added CMB data as a function of the 2GD wavelet half-width in a range corresponding to angular sizes between  $27.5'$  and  $30^\circ$  on the celestial sphere. Data (black rhombi) are compared with percentiles established from ten thousand statistically isotropic and Gaussian simulations produced from the concordance cosmological model. Significance levels lie roughly below 1.4% at the four wavelet scales  $a_8$ ,  $a_9$ ,  $a_{10}$ , and  $a_{11}$ , respectively corresponding to angular sizes of  $8.33^\circ$ ,  $10^\circ$ ,  $11.7^\circ$ , and  $13.3^\circ$ . The significance level reaches a minimum value of 0.49% at scale  $a_9$ . This identifies a strong detection of non-Gaussianity, in terms of an excess of kurtosis in the signed-intensity.

2004), leaving  $N_a$  valid pixels from which statistics may be estimated.

### 3.2 Non-Gaussianity analysis

The results of the application of the non-Gaussianity analysis of the local orientation, signed-intensity, and elongation to the three-year WMAP co-added CMB map are as follows. Let us recall that 17 scales of the 2GD wavelet are probed, corresponding to angular sizes on the celestial sphere between  $27.5'$  and  $30^\circ$ . The complete list of the wavelet half-widths  $\theta_{hw}$  considered in arcminutes reads:  $\{13.7', 25', 50', 75', 100', 150', 200', 250', 300', 350', 400', 450', 500', 550', 600', 750', 900'\}$ .

Firstly, the significance levels observed for statistics of the local orientation and of the local elongation reach minimum values between 5% and 10%, and only at some isolated scales. In other words, these values lie well inside the middle region defined above for the distribution of percentiles around the median value. We therefore conclude that no detection is obtained neither for the local orientation nor for the local elongation.

Secondly, the significance levels observed for the excess kurtosis of the signed-intensity are roughly below 1.4% at the four wavelet scales  $a_8$ ,  $a_9$ ,  $a_{10}$ , and  $a_{11}$ , respectively corresponding to angular sizes of  $8.33^\circ$ ,  $10^\circ$ ,  $11.7^\circ$ , and  $13.3^\circ$  on the celestial sphere. The excess kurtosis in the signed-intensity of the data at each of these wavelet scales is higher than the median value defined by the simulations. The significance level reaches a minimum value of 0.49% at scale  $a_9$ . These results identify a strong detection of non-Gaussianity in the WMAP co-added CMB data, in terms of an excess of

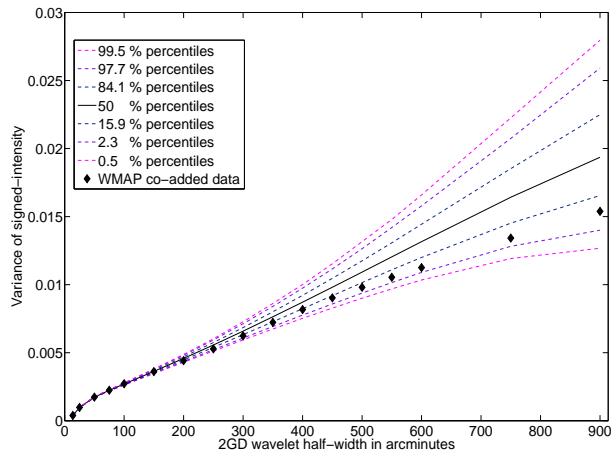


**Figure 2.** Variance of the signed-intensity of the three-year WMAP co-added CMB data as a function of the 2GD wavelet half-width in a range corresponding to angular sizes between  $27.5'$  and  $30^\circ$  on the celestial sphere. Data (black rhombi) are compared with percentiles established from ten thousand statistically isotropic and Gaussian simulations produced from the concordance cosmological model. Significance levels lie roughly above 5% between the wavelet scales  $a_2$  and  $a_{17}$ , corresponding to angular sizes between  $50'$  and  $30^\circ$ . At the wavelet scale  $a_1$  though, corresponding to an angular size of  $27.5'$ , the significance level reaches 0%. This identifies a strong, but isolated detection of non-Gaussianity, in terms of a too high variance of the signed-intensity.

kurtosis in the signed-intensity (see Figure 1). Also notice significance levels of roughly 1.6% and 1.2%, respectively at the wavelets scales  $a_4$  and  $a_5$ , corresponding to angular sizes of  $2.5^\circ$  and  $3.33^\circ$ . The excess kurtosis in the signed-intensity of the data at each of these wavelet scales is well lower than the median value defined by the simulations, even though it is not considered as anomalous.

Thirdly, the significance levels observed for the variance of the signed-intensity are roughly above 5% between the wavelet scales  $a_2$  and  $a_{17}$ , corresponding to angular sizes between  $50'$  and  $30^\circ$ , the minimum value being reached at scale  $a_8$ . Again, these values lie well inside the middle region defined above for the distribution of percentiles around the median value. We therefore conclude that no detection is obtained at those scales. At the wavelet scale  $a_1$  though, corresponding to an angular size of  $27.5'$ , the value of the variance is well higher than the median value defined by the simulations, and the significance level actually reaches 0%. Formally, this represents a strong, but isolated detection of non-Gaussianity in the WMAP co-added CMB data, in terms of a too high variance of the signed-intensity (see Figure 2). In Section 4, we suggest that it might originate in the presence of residual point sources in the data, and that it should therefore be discarded. Notice that no detection appears neither in the mean nor in the skewness of the signed-intensity.

In summary, the 2GD wavelet gives access to the measures of orientation, signed-intensity, and elongation of local features of the WMAP temperature data. But a strong detection of non-Gaussianity is only observed in the excess kurtosis of the signed-intensity. This result actually sup-

ports the previous detection, with the axisymmetric Mexican hat wavelet, of an excess of kurtosis in the wavelet coefficient of the WMAP temperature data (Vielva et al. 2004; Mukherjee & Wang 2004; Cruz et al. 2005).

## 4 SYSTEMATIC EFFECTS

In this section, we firstly suggest that the high variance of the signed-intensity of the WMAP temperature data at the smallest wavelet scales, and the corresponding isolated detection, might originate in the presence of residual point sources in the data. Secondly, we discard instrumental noise, residual foreground emissions, and large-scale modulations of the CMB temperature field related to some unknown systematics, as possible origins of the excess of kurtosis in the signed-intensity.

### 4.1 Residual point sources and lower resolution

The variance of the signed-intensity of the WMAP co-added CMB data is lower than the median value defined by the simulations between the wavelet scales  $a_6$  and  $a_{17}$ , corresponding to angular sizes between  $5^\circ$  and  $30^\circ$ . This variance is not considered as anomalous though, as significance levels are always roughly above 5%. On the contrary, the variance observed between the wavelet scales  $a_1$  and  $a_5$ , corresponding to angular sizes between  $27.5'$  and  $3.33^\circ$ , is higher than the median value. Again, the values of the variance between the wavelet scales  $a_2$  and  $a_5$  are not considered as anomalous, as significance levels are always roughly above 6%. As already emphasized, at the wavelet scale  $a_1$ , the significance level reaches 0%. The high variance at the smallest wavelet scales, in opposition with the behaviour at larger wavelet scales (see Figure 2), might originate in systematic effects such as the presence of residual point sources. Let us recall that the three-year WMAP best-fit angular power spectrum is obtained after correction for a non-zero best-fit amplitude of a residual point sources power spectrum (Hinshaw et al. 2007). Consistently, residual point sources were recently identified in the WMAP co-added CMB data (López-Cañiego et al. 2007). These residual point sources are however not accounted for in the WMAP co-added CMB data analyzed here, while they are accounted for in the simulations based on the three-year WMAP best-fit angular power spectrum. This could indeed explain the high variance observed in the signed-intensity of the data at the smallest wavelet scales. Obviously, the contribution of these residual point sources is negligible at larger wavelet scales.

In the absence of a detailed model of the contribution of the residual point sources to the variance of the signed-intensity, the corresponding isolated detection at the wavelet scale  $a_1$  is discarded, and the analysis is restricted to the wavelet scales between  $a_6$  and  $a_{17}$ , corresponding to angular sizes between  $5^\circ$  and  $30^\circ$ . This does not affect the interpretation of the detection relative to the excess kurtosis in the signed-intensity, which appears between the wavelet scales  $a_8$  and  $a_{11}$ , corresponding to angular sizes between  $8.33^\circ$  and  $13.3^\circ$ . For the subsequent analyses dedicated to search for the origin of the detection in the excess kurtosis of the signed-intensity, the three-year WMAP co-added CMB map

and the corresponding ten thousand simulations are downgraded to the resolution  $N_{side} = 32$ . This provides maps with a bit more than twelve thousand equal-area pixels with a spatial resolution of  $1.83^\circ$ . For coherence, the initial non-Gaussianity analysis is reproduced for the signed-intensity, from the data and simulations preliminary downgraded to the resolution  $N_{side} = 32$ . All conclusions relative to the first four statistical moments remain obviously unchanged. The strong detection in the excess kurtosis is slightly enhanced. The corresponding significance levels are roughly below 1% at the four wavelet scales  $a_8$ ,  $a_9$ ,  $a_{10}$ , and  $a_{11}$ , respectively corresponding to angular sizes of  $8.33^\circ$ ,  $10^\circ$ ,  $11.7^\circ$ , and  $13.3^\circ$  on the celestial sphere. The significance level reaches a minimum value of 0.26% at scale  $a_8$ .

### 4.2 Other systematics

Let us recall the previous detection of an excess of kurtosis in the wavelet coefficient of the WMAP temperature data with the axisymmetric Mexican hat wavelet (Vielva et al. 2004; Mukherjee & Wang 2004; Cruz et al. 2005), as well as previous detections of anomalies obtained in the signed-intensity of the WMAP temperature data with the 2GD wavelet (McEwen et al. 2007; Vielva et al. 2007). The corresponding analyses concluded that neither instrumental noise nor residual foreground emissions are at the origin of the deviations observed. These conclusions were drawn from independent analyses of the data produced by the eight WMAP radiometers at the Q, V, and W frequencies. These results suggest that the wavelets and statistics used are rather insensitive to instrumental noise and residual foreground emissions in the WMAP temperature data. In this context, even though no similar analysis is performed here, we conclude that neither instrumental noise nor residual foreground emissions are likely to be at the origin of the excess of kurtosis observed in the signed-intensity of the WMAP temperature data.

Further investigations are proposed here, considering some possible form of unknown systematics. It was recently proposed that the WMAP data are possibly affected by a large-scale modulation. This modulation was primarily put forward as a possible explanation of the North-South asymmetry and low multipoles alignment of the WMAP data (Helling et al. 2006; Gordon 2007). In that framework, the WMAP data are of the form  $T(\omega) \times [1 + f(\omega)]$ , where  $T(\omega)$  stands for the CMB temperature on the sky, and  $f(\omega)$  is a modulation function containing only low multipoles  $l$ . Dipolar ( $l = 1$ ) and dipolar-quadrupolar ( $l = \{1, 2\}$ ) modulation functions providing the best-fit cosmological models to the three-year WMAP data were proposed. Let us remark that the best-fit dipolar modulation used (Eriksen et al. 2007), as well as the best-fit dipolar-quadrupolar modulation used Spergel et al. (2007, see arXiv:astro-ph/0603449v1), were not primarily computed for the three-year WMAP co-added CMB map itself, but they were shown not to be sensitive to the three-year WMAP data set and sky cut. We therefore also considered them to be adequate for correction of the three-year WMAP co-added CMB map.

We have checked the stability of the excess of kurtosis in the signed-intensity of the three-year WMAP co-added CMB data relative to these modulations. Firstly, considering the best-fit dipolar-quadrupolar modulation, the strong

detection in the excess kurtosis remains unchanged, if it is not slightly increased. Just as for the analysis of the non-corrected three-year WMAP co-added CMB data, the significance levels are roughly below 1% at the four wavelet scales  $a_8$ ,  $a_9$ ,  $a_{10}$ , and  $a_{11}$ , respectively corresponding to angular sizes of  $8.33^\circ$ ,  $10^\circ$ ,  $11.7^\circ$ , and  $13.3^\circ$  on the celestial sphere. The significance levels reach a minimum value of 0.22% at scales  $a_8$  and  $a_9$ . Secondly, considering the best-fit dipolar modulation, the detection in the excess kurtosis is slightly decreased. The significance levels are only roughly below 3% at the four wavelet scales  $a_8$ ,  $a_9$ ,  $a_{10}$ , and  $a_{11}$ , with a minimum value of 0.60% at scale  $a_8$ . As already emphasized (Vielva et al. 2007), a more precise definition of the modulation in terms of specific systematic effects would be required before strong conclusions can be drawn from the application of the corresponding corrections. But, even taking the results at face value, the proposed dipolar and dipolar-quadrupolar corrections are to be rejected as possible origins of the observed excess of kurtosis in the signed-intensity of the WMAP temperature data.

In summary, instrumental noise and residual foreground emissions are not likely to be at the origin of the excess of kurtosis. Large-scale modulations of the CMB related to some unknown systematics are explicitly rejected as possible origins of the detection. The non-Gaussianity detected in the excess kurtosis of the signed-intensity of the WMAP data is therefore probably related to the CMB temperature field itself.

## 5 CONFINEMENT AND DISCUSSION

We here firstly recall the recent detection of an anomalous distribution on the sky of anomalous signed-intensities in the three-year WMAP co-added CMB data. We secondly test, and tend to reject, the possible confinement of the observed excess of kurtosis to the directions with an anomalous signed-intensity. We finally discuss the detailed interpretation of our detections.

### 5.1 Local signed-intensity anomalies

In a very recent analysis of the three-year WMAP co-added CMB data with the 2GD wavelet, the distribution on the celestial sphere of directions with a signed-intensity anomalous at 99.865% (formally corresponding to the percentiles at three standard deviations ( $3\sigma$ ) from the mean in a Gaussian distribution) was observed to be anomalous (Vielva et al. 2007). At the wavelet scale  $a_8$ , corresponding to an angular size of  $8.33^\circ$ , the global significance level of that detection, defined as the fraction of the ten thousand simulations with a number of anomalous directions higher than in the data, is 1.39%. The anomalous directions are essentially distributed in three clusters in the southern galactic hemisphere, identifying three mean preferred directions in the sky Vielva et al. (2007, Figure 5). A first cold spot (*i.e.* with negative signed-intensities) identifies with the anomalous cold spot originally detected at  $(\theta, \varphi) = (147^\circ, 209^\circ)$  in galactic spherical coordinates with the axisymmetric Mexican hat wavelet (Vielva et al. 2004; Cruz et al. 2005). A second cold spot lies very close to the southern end of the CMB dipole axis. The third spot is a hot spot (*i.e.* with positive

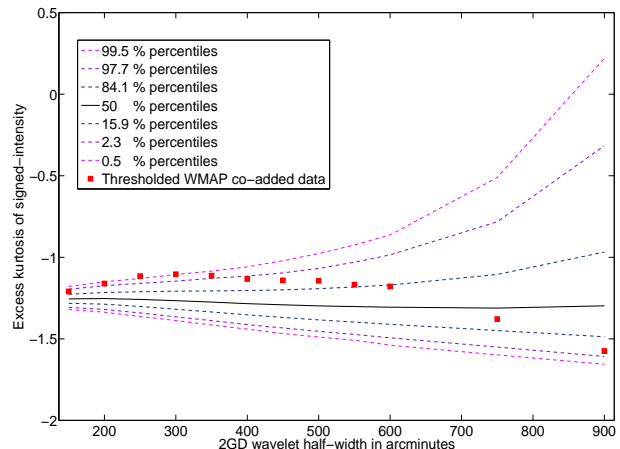


**Figure 3.** Excess kurtosis of the signed-intensity of the three-year WMAP co-added CMB data as a function of the 2GD wavelet half-width in a range corresponding to angular sizes between  $5^\circ$  and  $30^\circ$  on the celestial sphere. Data (red squares) are compared with percentiles established from ten thousand statistically isotropic and Gaussian simulations produced from the concordance cosmological model. The directions with an anomalous signed-intensity are excluded from the statistical analysis, in the data as well as in each of the ten thousand simulations independently. Significance levels are roughly below 1% at the four wavelet scales  $a_7$ ,  $a_8$ ,  $a_9$ , and  $a_{10}$ , respectively corresponding to angular sizes of  $6.67^\circ$ ,  $8.33^\circ$ ,  $10^\circ$ , and  $11.7^\circ$ . The significance level reaches a minimum value of 0.28% at scale  $a_8$ . This still identifies a strong detection of non-Gaussianity, in terms of an excess of kurtosis in the signed-intensity.

signed-intensities) close to the southern end of the ecliptic poles axis. The detection is confirmed at the neighbour wavelet scales  $a_9$ ,  $a_{10}$ , and  $a_{11}$ , respectively corresponding to angular sizes of  $10^\circ$ ,  $11.7^\circ$ , and  $13.3^\circ$ . Instrumental noise, residual foreground emissions, as well as large-scale modulations of the CMB related to some unknown systematics, are rejected as possible origins of the detection. The localized anomalous distribution of anomalous signed-intensities identified may therefore probably be imputed to the CMB temperature field itself.

### 5.2 Confinement analysis

Postulating the Gaussianity of the CMB, one may interpret the anomalous distribution of directions with an anomalous signed-intensity as a clear departure from statistical isotropy (Vielva et al. 2007). But more generally, the anomaly observed highlights a deviation of the CMB temperature field from the whole assumption of statistical isotropy and Gaussianity. In the context of the present non-Gaussianity detection, the anomalous distribution of anomalous signed-intensities previously identified represents a serious candidate to explain the excess of kurtosis observed in the signed-intensity of the three-year WMAP co-added CMB data. This idea is supported by the fact that the two detections are observed at the same wavelet scales. The hypothesis to check is to know if the whole non-Gaussianity observed is confined to the directions with an anomalous signed-intensity, in the idea that the excess in the number of anomalous directions would bear the departure from Gaussianity.

The confinement analysis simply consists in reproducing the previous analysis on the first four statistical moments of the signed-intensity of the three-year WMAP co-added CMB data, from which the directions with an anomalous signed-intensity are excluded. The only way to account for a possible bias introduced by the exclusion of the extremal values of the data above a given threshold is to apply the same exclusion process to each simulation independently. In particular, the coherence of the procedure can only be achieved if all values above the threshold, and not only part of it, are identified and excluded from the statistical analysis, in the data and in the simulations<sup>4</sup>. Notice that, while the anomalous signed-intensities were originally identified at a threshold of 99.865%, we consider here a threshold at 99.5%. This lowering is performed in order to avoid a possible negative conclusion, relative to the confinement, simply due to the fact that directions in the immediate vicinity of the directions thresholded are not excluded from the analysis. For completeness, even though the detections are only observed at the four wavelet scales between  $a_8$  and  $a_{11}$ , corresponding to angular sizes between  $8.33^\circ$  and  $13.3^\circ$ , the confinement analysis is performed at all wavelet scales between  $a_6$  and  $a_{17}$ , corresponding to angular sizes between  $5^\circ$  and  $30^\circ$ .

The results of the analysis performed are as follows. The strong detection of an excess of kurtosis in the signed-intensity of the WMAP temperature data is preserved. The significance levels are roughly below 1% at the four wavelet scales  $a_7$ ,  $a_8$ ,  $a_9$ , and  $a_{10}$ , respectively corresponding to angular sizes of  $6.67^\circ$ ,  $8.33^\circ$ ,  $10^\circ$ , and  $11.7^\circ$  on the celestial sphere. The significance level reaches a minimum value of 0.28% at scale  $a_8$  (see Figure 3). The variance of the signed-intensity at each wavelet scale was well lower than the median value defined by the simulations before the thresholding. It was not considered as anomalous as the significance level reached a minimum value of roughly 5% at scale  $a_8$ . The variance of the signed-intensity at each wavelet scale is still well lower than the median value defined by the simulations after the thresholding. It is still not considered as anomalous, even though the significance level reaches a minimum value of roughly 1% at scale  $a_8$ . No detection appears neither in the mean nor in the skewness of the signed-intensity.

In summary, removing the directions with an anomalous signed-intensity does not solve the observed discrepancy between the WMAP temperature data and simulations. Consequently, taking the CMB temperature angular power spectrum of the concordance cosmological model at face value, we can conclude that the strong detection in the excess kurtosis of the signed-intensity of the WMAP temperature data is not confined to the directions with an anomalous signed-intensity.

<sup>4</sup> We therefore have to assume that, in the data, all extremal values of the background Gaussian distribution above the threshold are excluded. The only formal reason for which extremal values outside the effectively observed directions with a signed-intensity above the threshold might have been missed would be that some non-Gaussianity coincidentally compensates for the extremal value in the corresponding direction on the celestial sphere. In that trivial case, one readily knows that the non-Gaussianity observed in the WMAP data is not confined to the localized distribution of anomalous signed-intensities.

### 5.3 Discussion

Firstly, if the excess of kurtosis observed in the signed-intensity of the WMAP temperature data is related to the CMB temperature field itself (see Section 4), the fact that this non-Gaussianity is not confined to the directions with an anomalous signed-intensity seems natural. Indeed, independently of the modification of the basic inflationary scenario that might explain the non-Gaussianity of the CMB temperature field (Bartolo et al. 2004), the cosmological principle still implies its statistical isotropy, at least as a first approximation. Non-Gaussian perturbations are therefore more naturally widely spread over the whole sky. We also notice that the wavelet scales at which the non-Gaussianity is observed are compatible with the size of CMB anisotropies due to topological defects such as cosmic textures (Turok & Spergel 1990), or due to the Integrated Sachs-Wolfe effect, which is associated with the time evolution of the gravitational potential of large scale structures (Sachs & Wolfe 1967; Rees & Sciama 1968; Martínez-González & Sanz 1990). Texture models suggest the presence of a number of textures with angular sizes above  $1^\circ$ , which can induce hot spots or cold spots of corresponding angular size in the CMB (Turok & Spergel 1990). A recent Bayesian analysis (Cruz et al. 2007) showed that the cold spot originally detected at  $(\theta, \varphi) = (147^\circ, 209^\circ)$  in galactic spherical coordinates with the axisymmetric Mexican hat wavelet, is satisfactorily described by a texture with an angular size on the celestial sphere around  $10^\circ$ . Other analyses also showed that the time evolution of the gravitational potential of large scale structures such as voids might induce cold spots in the CMB with angular sizes of several degrees on the celestial sphere (Martínez-González & Sanz 1990). The cold spot identified at  $(\theta, \varphi) = (147^\circ, 209^\circ)$  in galactic spherical coordinates with an angular size around  $10^\circ$  could actually be explained in terms of a void at a redshift  $z \simeq 1$  and with a diameter around  $300h^{-1}$  Mpc (Inoue & Silk 2006, 2007; Rudnick et al. 2007).

Secondly, as already emphasized, an excess of kurtosis in the wavelet coefficient of the WMAP temperature data was previously detected with the axisymmetric Mexican hat wavelet. The non-Gaussian deviation observed with the axisymmetric Mexican hat wavelet is undoubtedly related to the present detection in the excess kurtosis of the signed-intensity with the 2GD wavelet, notably because it is observed with a similar statistics at the same angular sizes on the celestial sphere. From this point of view, both detections support one another. But the axisymmetric Mexican hat wavelet also allowed the detection of the cold spot at  $(\theta, \varphi) = (147^\circ, 209^\circ)$  in galactic spherical coordinates, which was interpreted to be the exclusive origin of the excess of kurtosis detected (Cruz et al. 2005). On the contrary, we have concluded that the detection in the excess kurtosis of the signed-intensity of the WMAP temperature data with the 2GD wavelet is not confined to the previously identified directions with an anomalous signed-intensity. Consequently, even though the two detections are similar, they probably simply do not identify the same non-Gaussian content in the WMAP temperature data.

Finally, let us also underline that the values of the cosmological parameters are affected by uncertainties associated with the limited precision of measurement of the CMB



temperature angular power spectrum. These uncertainties are associated with the cosmic variance, but also with systematic effects such as instrumental noise and residual foreground emissions. The simulations produced for our analysis are obtained from the angular power spectrum determined by the cosmological parameters of the concordance model (*i.e.* the three-year WMAP best-fit model). They do not account for the quoted uncertainties. Consequently, before giving full credit to our conclusions, a deep analysis should be performed to check the stability of the various detections considered when the WMAP temperature data are compared with simulations produced from any possible angular power spectrum inside the experimental error bars. Formally, any of our conclusions might be affected by this further analysis, from the fact that the non-Gaussianity observed in the WMAP temperature data is not confined to the directions with an anomalous signed-intensity, up to the mere detection of an excess of kurtosis in the signed-intensity. However, such an analysis would be very involved and is not produced here. On the one hand, the stability of the detection of an excess of kurtosis in the wavelet coefficient of the WMAP temperature data with the axisymmetric Mexican hat wavelet was suggested (Vielva et al. 2004). The same conclusion probably holds for the present detection of an excess of kurtosis in the signed-intensity of the WMAP temperature data with 2GD wavelet. On the other hand, the confinement analysis itself is based on the previous detection of the distribution of directions with an anomalous signed-intensity (Vielva et al. 2007). At present, no analysis confirmed the stability of this distribution relative to the uncertainties on the cosmological parameters. A possible excess of power in the concordance model relative to the WMAP temperature data (Spergel et al. 2003; Hinshaw et al. 2007; Monteserín et al. 2007) might imply that a part of the distribution on the celestial sphere of directions with an anomalous signed-intensity was actually not detected. This would probably not question the fact that this distribution is anomalous at the wavelet scales between  $a_8$  and  $a_{11}$ , corresponding to angular sizes between  $8.33^\circ$  and  $13.3^\circ$ , but would simply suggest that the global significance level for the detection was underestimated. However in such a case, the confinement analysis itself, which explicitly requires the exclusion of all the extremal values above a given threshold, both in the data and in the simulations, might not be performed anymore. No conclusion relative to the possible confinement of the non-Gaussianity observed to the directions with an anomalous signed-intensity could therefore be reached.

## 6 CONCLUSION

The decomposition of a signal on the sphere with the steerable wavelet constructed from the second Gaussian derivative gives access to morphological measures such as the orientation, signed-intensity, and elongation of the signal's local features. In this work, the three-year WMAP co-added data of the CMB temperature field are analyzed through the first four statistical moments of the random fields associated with these local morphological measures, at wavelet scales corresponding to angular sizes between  $27.5'$  and  $30^\circ$  on the celestial sphere. The statistical analysis is performed

by comparison of the data with ten thousand statistically isotropic and Gaussian simulations produced from the concordance cosmological model. No detection is made neither in the orientation analysis nor in the elongation analysis. A strong detection is made in the excess kurtosis of the signed-intensity of the WMAP data, with a significance level below 0.5% at a wavelet scale corresponding to an angular size around  $10^\circ$ , and confirmed at neighbour scales. This supports a previous detection of an excess of kurtosis in the wavelet coefficient of the WMAP data with the axisymmetric Mexican hat wavelet. An isolated detection is also made in the variance of the signed-intensity at the smallest wavelet scale. Systematic effects such as residual point sources in the WMAP co-added CMB data are suggested to originate this anomaly, which is consequently simply discarded.

Instrumental noise and residual foreground emissions are not likely to be at the origin of the detection in the excess kurtosis of the signed-intensity. Large-scale modulations of the CMB related to some unknown systematics are explicitly rejected as possible origins of the detection. The observed non-Gaussianity is therefore probably to be imputed to the CMB temperature field itself, thereby questioning the basic inflationary scenario upon which the concordance cosmological model relies. In this context, taking the CMB temperature angular power spectrum of the concordance cosmological model at face value, further analysis also naturally suggests that this non-Gaussianity of the WMAP temperature data is not confined to the localized distribution of anomalous signed-intensities. However, this last result, in particular, might be sensitive to uncertainties affecting the cosmological parameters. Further analyses should be performed before giving it full credit.

## ACKNOWLEDGMENTS

The work of Y.W. is funded by the Swiss National Science Foundation (SNF) under contract No. 200021-107478/1. Y.W. is also postdoctoral researcher of the Belgian National Science Foundation (FNRS). The work of P.V. is funded through an I3P contract from the Spanish National Research Council (CSIC). P.V., R.B.B., and E.M.-G. are also supported by the Spanish MCYT project ESP2004-07067-C03-01. The authors acknowledge the use of the Legacy Archive for Microwave Background Data Analysis (LAMBDA). Support for LAMBDA is provided by the NASA Office of Space Science. The authors also acknowledge the use of the HEALPix and CAMB softwares.

## REFERENCES

- Abramo L.R., Bernui A., Ferreira I.S., Villela T., Wuensche C.A., 2006, Phys. Rev. D, 74, 063506
- Bartolo N., Komatsu E., Matarrese S., Riotto A., 2004, Phys. Rep., 402, 103
- Bennett C.L. et al., 2003, ApJS, 148, 1
- Bernui A., Villela T., Wuensche C.A., Leonardi R., Ferreira I., 2006, A&A, 454, 409
- Bernui A., Mota B., Rebouças M.J., Tavakol R., 2007, A&A, 464, 479

- Bielewicz P., Eriksen H.K., Banday A.J., Grski K.M., Lilje P.B., 2005, *ApJ*, 635, 750
- Cayón L., Jin J., Treaster A., 2005, *MNRAS*, 362, 826
- Chiang L.-Y., Naselsky P.D., Verkhodanov O.V., Way M.J., 2003, *ApJ*, 590, L65
- Chiang L.-Y., Naselsky P.D., 2006, *Int. J. Mod. Phys D*, 15, 1283
- Coles P., Dinnen P., Earl J., Wright D., 2004, *MNRAS*, 350, 983
- Copi C.J., Huterer D., Starkman G.D., 2004, *Phys. Rev. D*, 70, 043515
- Cruz M., Martínez-González E., Vielva P., Cayn L., 2005, *MNRAS*, 356, 29
- Cruz M., Tucci M., Martínez-González E., Vielva P., 2006, *MNRAS*, 369, 57
- Cruz M., Cayn L., Martínez-González E., Vielva P., Jin J., 2007a, *ApJ*, 655, 11
- Cruz M., Turok N., Vielva P., Martínez-González E., Hobson M.P., 2007b, *Science*, 318, 1612
- de Oliveira-Costa A., Tegmark M., Zaldarriaga M., Hamilton A., 2004, *Phys. Rev. D*, 69, 063516
- Donoghue E.P., Donoghue J.F., 2005, *Phys. Rev. D*, 71, 043002
- Eriksen H.K., Hansen F.K., Banday A.J., Grski K.M., Lilje P.B., 2004a, *ApJ*, 605, 14
- Eriksen H.K., Novikov D.I., Lilje P.B., Banday A.J., Górski K.M., 2004b, *ApJ*, 612, 64
- Eriksen H.K., Banday A.J., Górski K.M., Lilje P.B., 2005, *ApJ*, 622, 58
- Eriksen H.K., Banday A.J., Górski K.M., Hansen F.K., Lilje P.B., 2007, *ApJ*, 660, L81
- Freeman P.E., Genovese C.R., Miller C.J., Nichol R.C., Wasserman L., 2006, *ApJ*, 638, 1
- Gordon C., 2007, *ApJ*, 656, 636
- Górski K.M., Hivon E., Banday A.J., Wandelt B.D., Hansen F.K., Reinecke M., Bartelmann M., 2005, *ApJ*, 622, 759
- Hansen F.K., Cabella P., Marinucci D., Vittorio N., 2004a, *ApJ*, 607, L67
- Hansen F.K., Banday A.J., Grski K.M., 2004b, *MNRAS*, 354, 641
- Helling R.C., Schupp P., Tesileanu T., 2006, *Phys. Rev. D*, 70, 063004
- Hinshaw G. et al., 2007, *ApJS*, 170, 288
- Inoue K.T., Silk J., 2006, *ApJ*, 648, 23
- Inoue K.T., Silk J., 2007, *ApJ*, 664, 650
- Katz G., Weeks J., 2004, *Phys. Rev. D*, 70, 063527
- Komatsu E. et al., 2003, *ApJS*, 148, 119
- Land K., Magueijo J., 2005a, *MNRAS*, 357, 994
- Land K., Magueijo J., 2005b, *Phys. Rev. Lett.*, 95, 071301
- Land K., Magueijo J., 2007, *MNRAS*, 378, 153
- Larson D.L., Wandelt B.D., 2004, *ApJ*, 613, L85
- Larson D.L., Wandelt B.D., 2005, preprint (arXiv:astro-ph/0505046v1)
- López-Cañiego M., González-Nuevo J., Herranz D., Mascardi M., Sanz J.L., De Zotti G., Toffolati L., Argeso F., 2007, *ApJS*, 170, 108
- Martínez-González E., Sanz J.L., 1990, *MNRAS*, 247, 473
- McEwen J.D., Hobson M.P., Lasenby A.N., Mortlock D.J., 2005, *MNRAS*, 259, 1583
- McEwen J.D., Hobson M.P., Lasenby A.N., Mortlock D.J., 2006, *MNRAS*, 371, 50
- McEwen J.D., Wiaux Y., Hobson M.P., Vanderghenst P., Lasenby A.N., 2007, *MNRAS*, in press (arXiv:0704.0626v1 [astro-ph])
- Monteserín C., Barreiro R.B., Vielva P., Martínez-González E., Hobson M.P., Lasenby A.N., 2007, preprint (arXiv:0706.4289v1 [astro-ph])
- Mukherjee P., Wang Y., 2004, *ApJ*, 613, 51
- Naselsky P.D., Chiang L.-Y., Olesen P., Novikov D.I., 2005, *Phys. Rev. D*, 72, 063512
- Park C.-G., 2004, *MNRAS*, 349, 313
- Rees M.J., Sciama D.W., 1968, *Nature*, 217, 511
- Rudnick L., Brown S., Williams L.R., 2007, 671, 40
- Sachs R.K., Wolfe A.M., 1967, *ApJ*, 147, 73
- Schwarz D.J., Starkman G.D., Huterer D., Copi C.J., 2004, *Phys. Rev. Lett.*, 93, 221301
- Spergel D.N. et al., 2003, *ApJS*, 148, 175
- Spergel D.N. et al., 2007, *ApJS*, 170, 377
- Tojeiro R., Castro P.G., Heavens A.F., Gupta S., 2006, *MNRAS*, 365, 265
- Turok N., Spergel D.N., 1990, *Phys. Rev. Lett.* 64, 2736
- Vielva P., Martínez-González E., Barreiro R.B., Sanz J.L., Cayn L., 2004, *ApJ*, 609, 22
- Vielva P., Wiaux Y., Martínez-González E., Vanderghenst P., 2006, *New Astron. Rev.*, 50, 880
- Vielva P., Wiaux Y., Martínez-González E., Vanderghenst P., 2007, *MNRAS*, 381, 932
- Wiaux Y., Jacques L., Vanderghenst P., 2005, *ApJ*, 632, 5
- Wiaux Y., Vielva P., Martínez-González E., Vanderghenst P., 2006a, *Phys. Rev. Lett.*, 96, 151303
- Wiaux Y., Jacques L., Vielva P., Vanderghenst P., 2006b, *ApJ*, 652, 820